Supplementary Materials for

Structure and evolution of Photosystem I in the early-branching cyanobacterium *Anthocerotibacter panamensis*

Authors

Han-Wei Jiang[1,†], Christopher J. Gisriel[2,3,†,*], Tanai Cardona[4,†], David A. Flesher[5], Gary W. Brudvig[2,5], Ming-Yang Ho[1,6,*]

Affiliations

[1]Department of Life Science, National Taiwan University, Taipei, Taiwan

[2]Department of Chemistry, Yale University, New Haven, CT, USA

[3]Department of Biochemistry, University of Wisconsin-Madison, Madison, WI, USA

[4]School of Biological and Behavioural Sciences, Queen Mary University of London, London, United Kingdom

[5]Department of Molecular Biophysics and Biochemistry, Yale University, New Haven, CT, USA

[6]Institute of Plant Biology, National Taiwan University, Taipei, Taiwan

*Correspondence: mingyang@ntu.edu.tw and gisriel@wisc.edu

†These authors contributed equally to this work

This PDF file includes:

Supplementary Figures

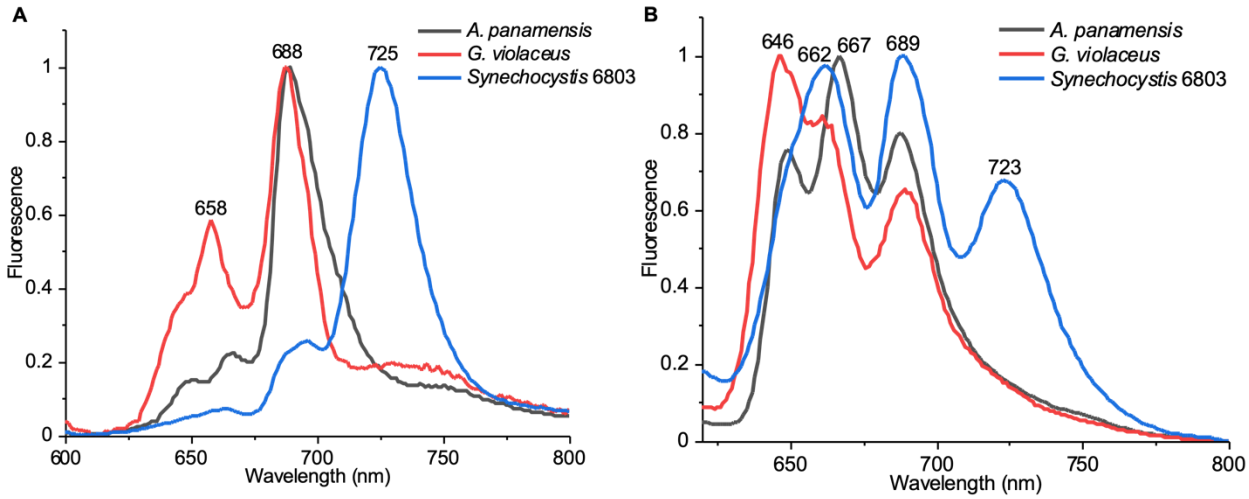

Fig. S1. Low temperature (77 K) fluorescence emission spectrum of *A. panamensis, G. violaceus*, and *Synechocystis* 6803 cells. (**A**) Excitation wavelength at 440 nm. (**B**) Excitation wavelength at 580 nm.

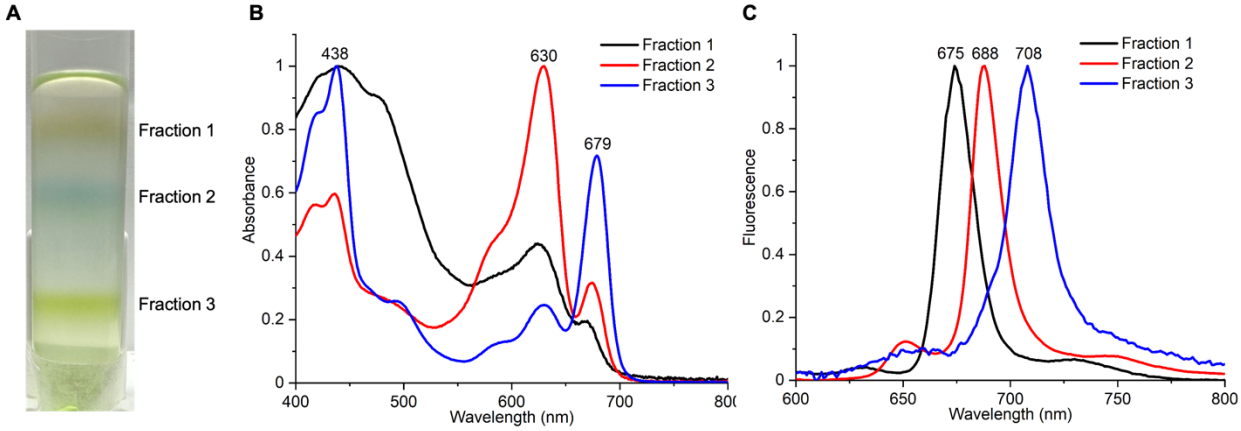

Fig. S2. Spectroscopic characterization of the PSI fractions from *A. panamensis*. (**A**) Separation of solubilized *A. panamensis* cell membranes by sucrose density gradient centrifugation. (**B**) Room-temperature absorption spectrum of sucrose gradient fractions. (**C**) 77 K fluorescence emission spectrum of sucrose gradient fractions excited at 440 nm.

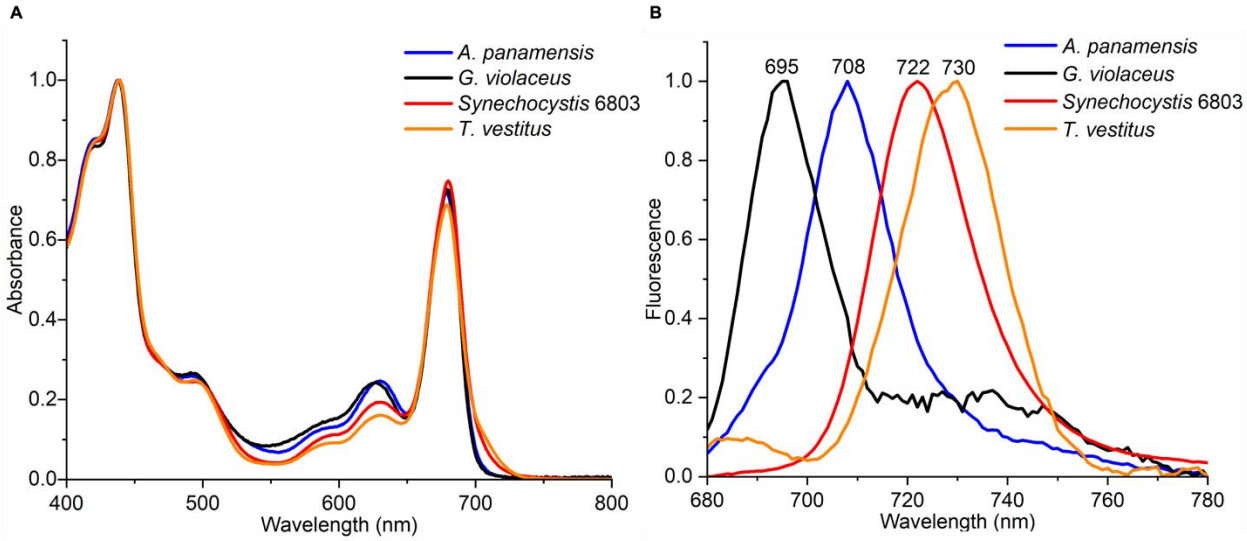

Fig. S3. Absorption spectra and 77 K fluorescence emission of PSI from *A. panamensis* (blue), *G. violaceus* (black), *Synechocystis* 6803 (red), and *T. vestitus* (orange). (**A**) Absorption spectra measured at room-temperature and normalized by their maximum peak intensities. (**B**) Fluorescence spectra measured at 77 K and normalized by their maximum peak intensities. The absorption spectra data and 77 K fluorescence-emission data of *T. vestitus* were adapted from Çoruh et al., 2021 (*25*).

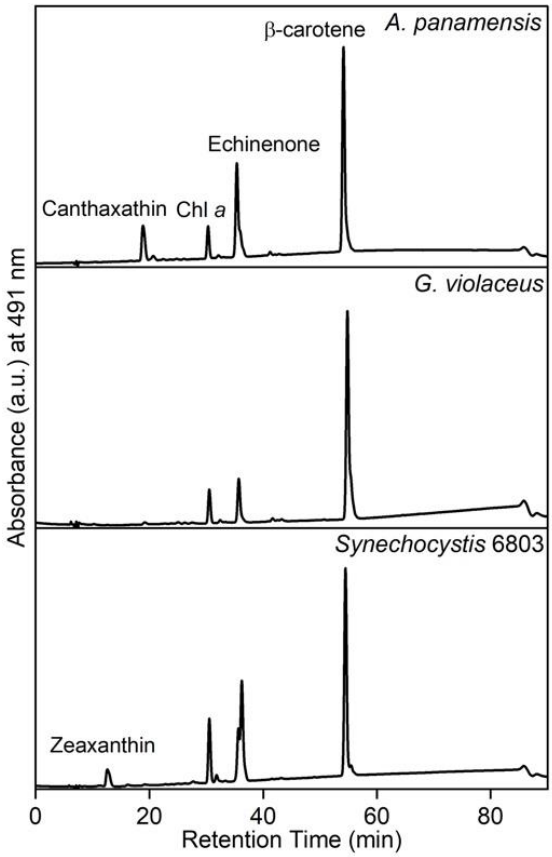

Fig. S4. HPLC analysis of PSI from *A. panamensis*, *G. violaceus*, and *Synechocystis* 6803. Four major pigment peaks are eluted from the PSI of *A. panamensis* and are identified as canthaxanthin, chlorophyll *a* (Chl *a*), echinenone, and β-carotene, respectively, based on their elution time and characteristic absorption spectra (**Fig. S5**).

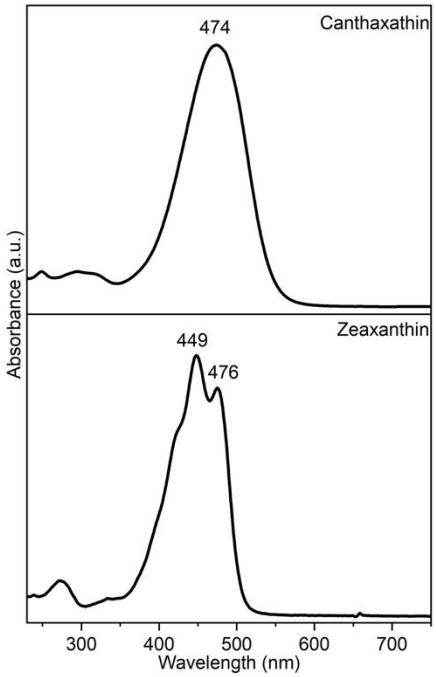

Fig. S5. The absorption spectra of components eluted in HPLC analysis. (A) Canthaxanthin in *A. panamensis*. **(B)** Zeaxanthin in *Synechocystis* 6803.

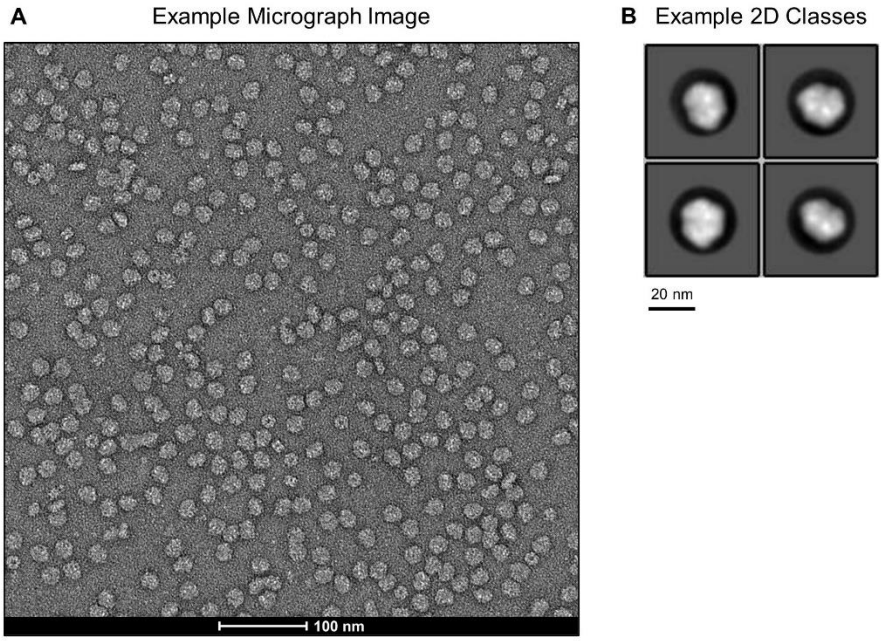

Fig. S6. TEM of negatively stained *A. panamensis* PSI. (**A**) Example micrograph. (**B**) Example 2D Classes.

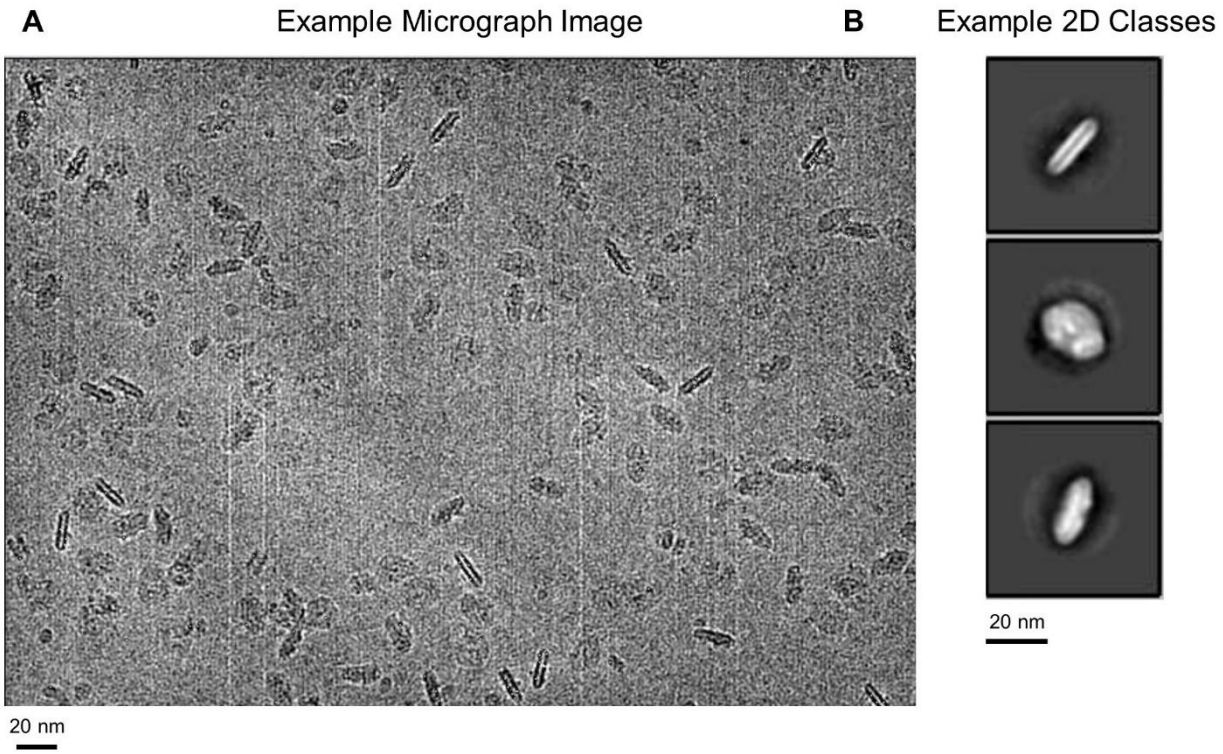

Fig. S7. Glacios cryo-EM screening of *A. panamensis* PSI. (**A**) Example micrograph. (**B**) Example 2D Classes.

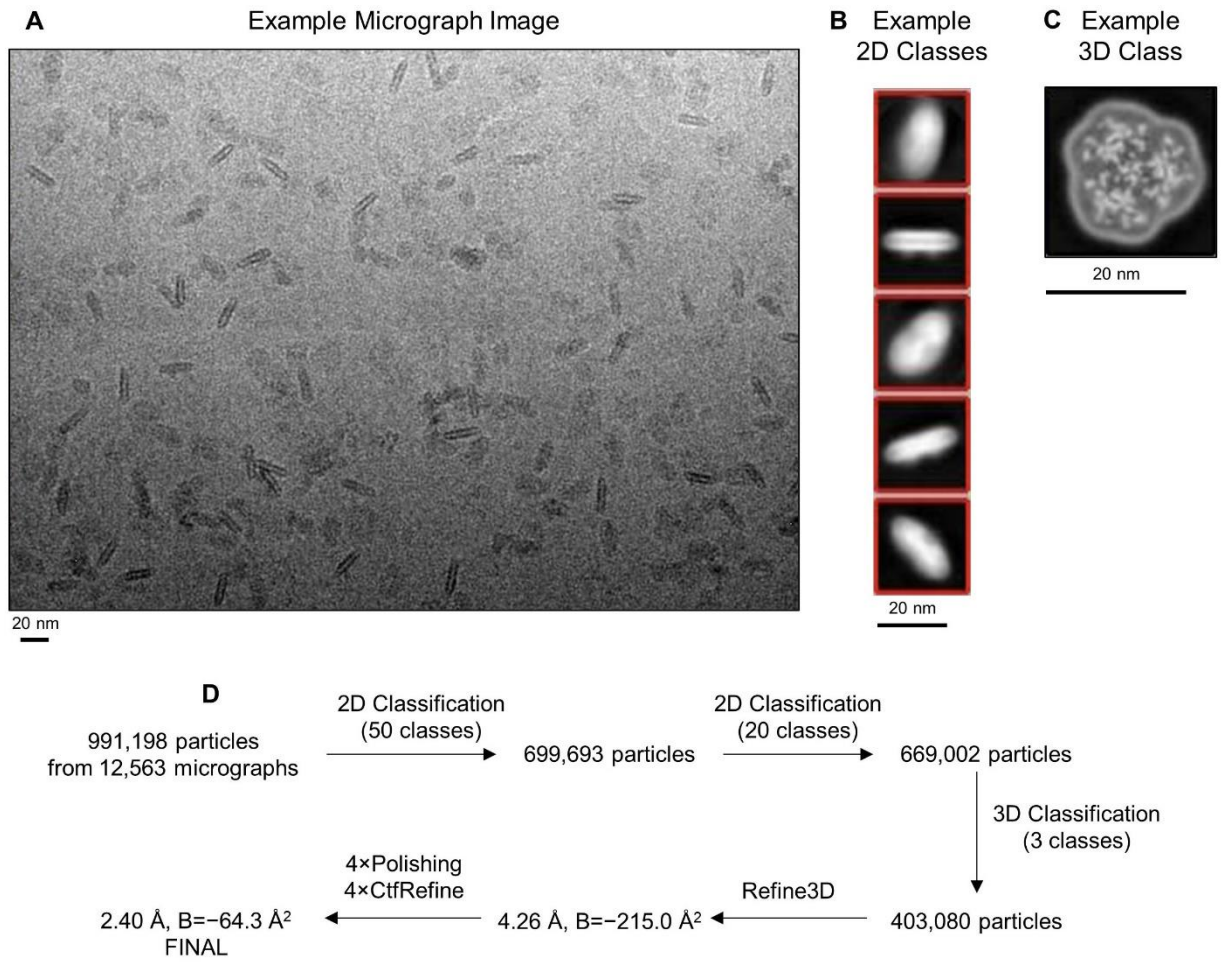

Fig. S8. Krios cryo-EM screening of *A. panamensis* PSI. (**A**) Example micrograph. (**B**) Example 2D Classes. (**C**) Example slice through a 3D class. (**D**) Overall workflow of data processing.

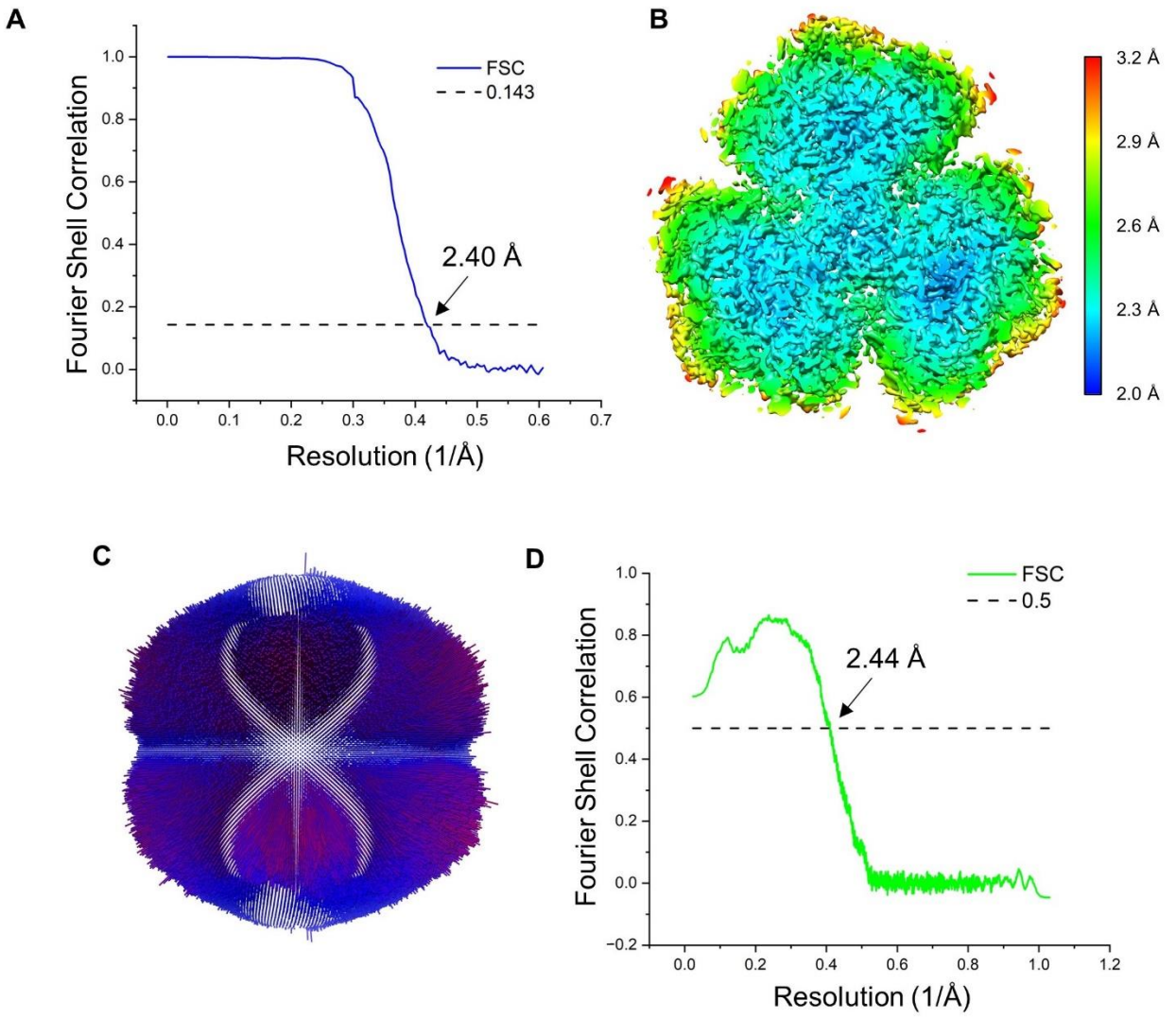

Fig. S9. Resolution and completeness of cryo-EM data. (**A**) Map-to-map Fourier Shell Correlation. (**B**) Local resolution map. (**C**) Angular distribution of the cryo-EM data. (**D**) Map-to-model Fourier Shell Correlation.

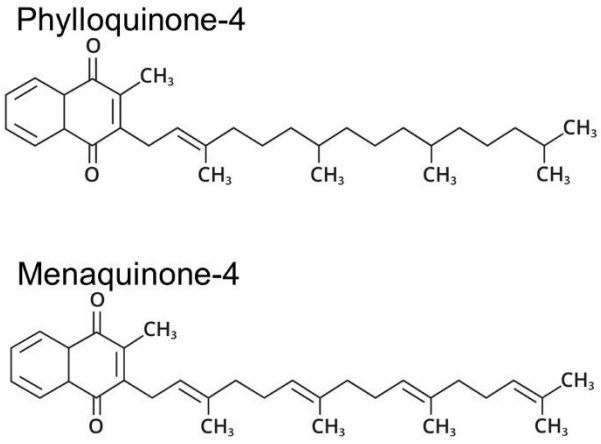

Fig. S10. Structures of PhQ-4 and MQ-4.

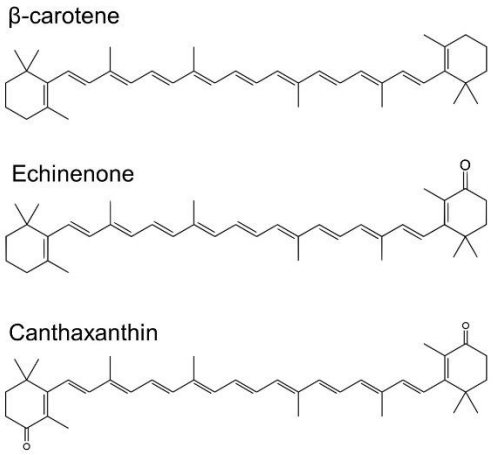

Fig. S11. Structures of β-carotene, echinenone, and canthaxanthin.

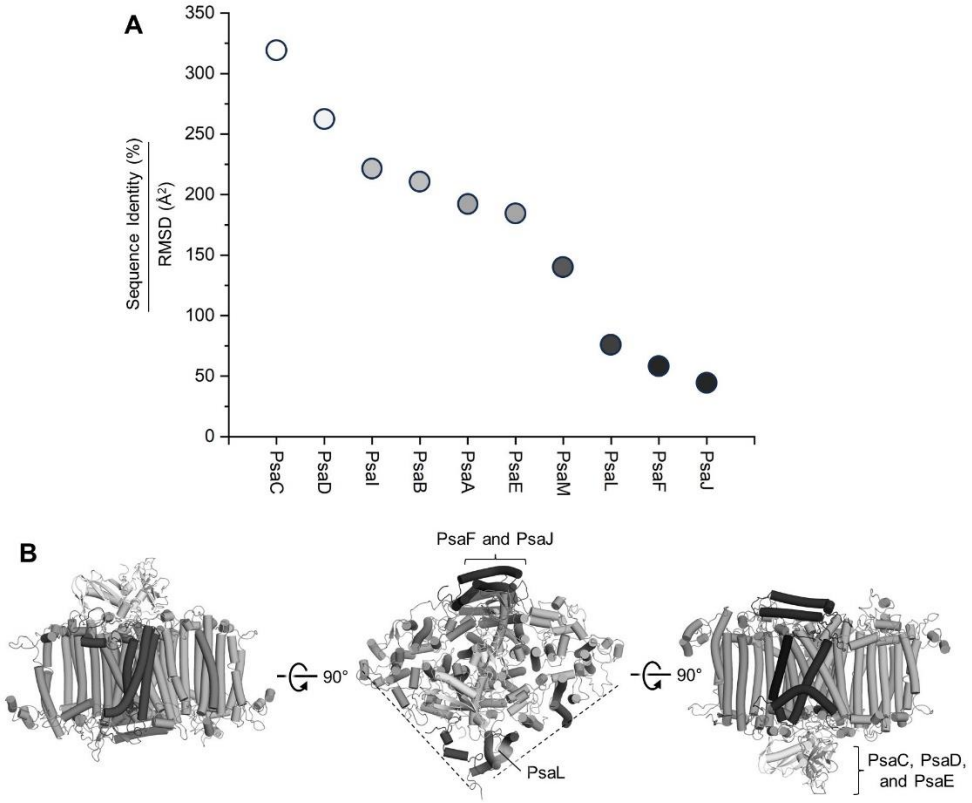

Fig. S12. Comparison of the *A. panamensis* PSI structure to *G. violaceus* PSI. (**A**) Plot of sequence identity (%) divided by RMSD (Å^2) for each subunit. (**B**) Structure of an *A. panamensis* PSI monomer where subunits are colored as the shades of circles in panel a. In the center panel, dashed lines correspond to monomer-monomer interfaces. Note that this table is generated from the data shown in **Table S3**.

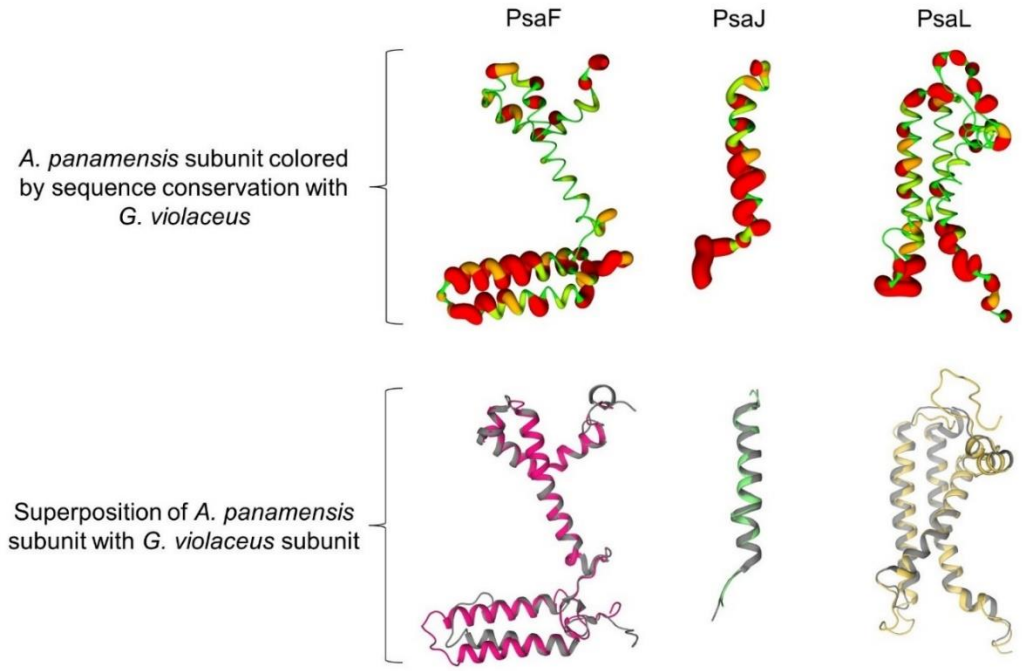

Fig. S13. Structural view of sequence conservation and superposition of selected *A. panamensis* PSI subunits with *G. violaceus* subunits.

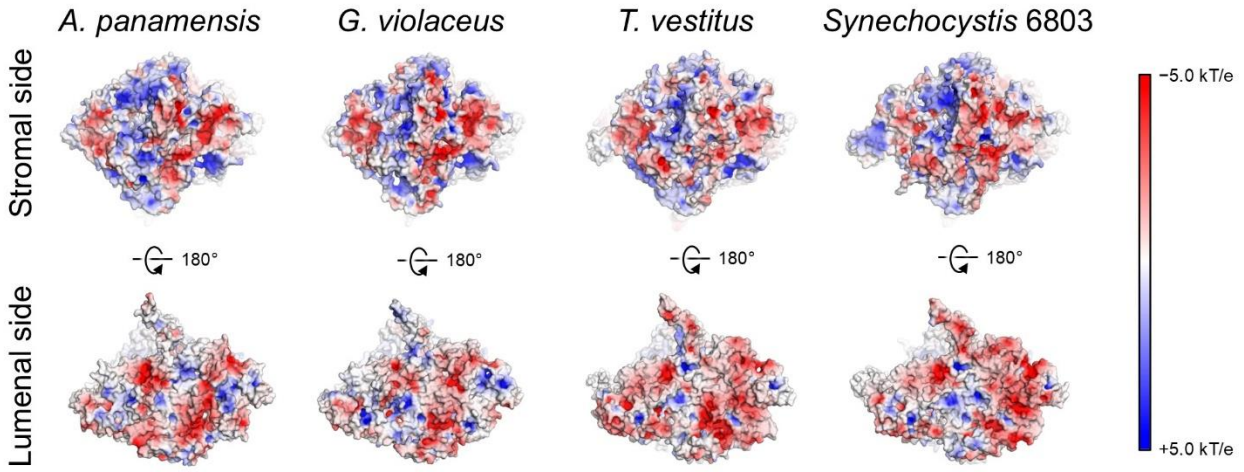

Fig. S14. Surface electrostatics comparison between selected PSI complexes. Note that the lumenal side of the PsaL region is more negatively charged in *T. vestitus* and *Synechocystis* 6803 compared to *A. panamensis* and *G. violaceus*.

A

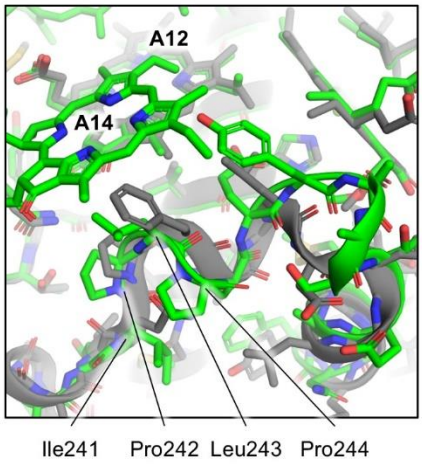

B

Ancestral PsaA	DIPLPHEFI	
PsaA *T. vestitus*	DIPLPHEFI 243	(has A14)
PsaA *Synechocystis* 6803	DIPLPHEFI 243	(has A14)
PsaA *A. panamensis*	DIPLPHEYA 248	(has A14)
PsaA *C. vandensis*	AIPLPHEYA 247	
PsaA ES-bin-313	EVVIP---G 244	
PsaA ES-bin-141	DVNPFL--G 256	
PsaA *G. violaceus*	QVNPFA--G 245	(lacks A14)
PsaA *G. morelensis*	QVNAFA--G 245	
PsaA *G. kilaueensis*	QVNPFL--G 345	

Fig. S15. Structural and sequence analysis of the A14/A12 Chl site. (**A**) Superposition of the *A. panamensis* and *G. violaceus* PSI structures in the vicinity of the A14/A12 Chl site. Residues conserved in *A. panamensis*, *T. vestitus*, and *Synechocystis* 6803 PSI are labeled. (**B**) Partial sequence alignment of PsaA in the vicinity of A14/A12. The Clustal Omega sequence identifiers are shown at the bottom of each position (*59*).

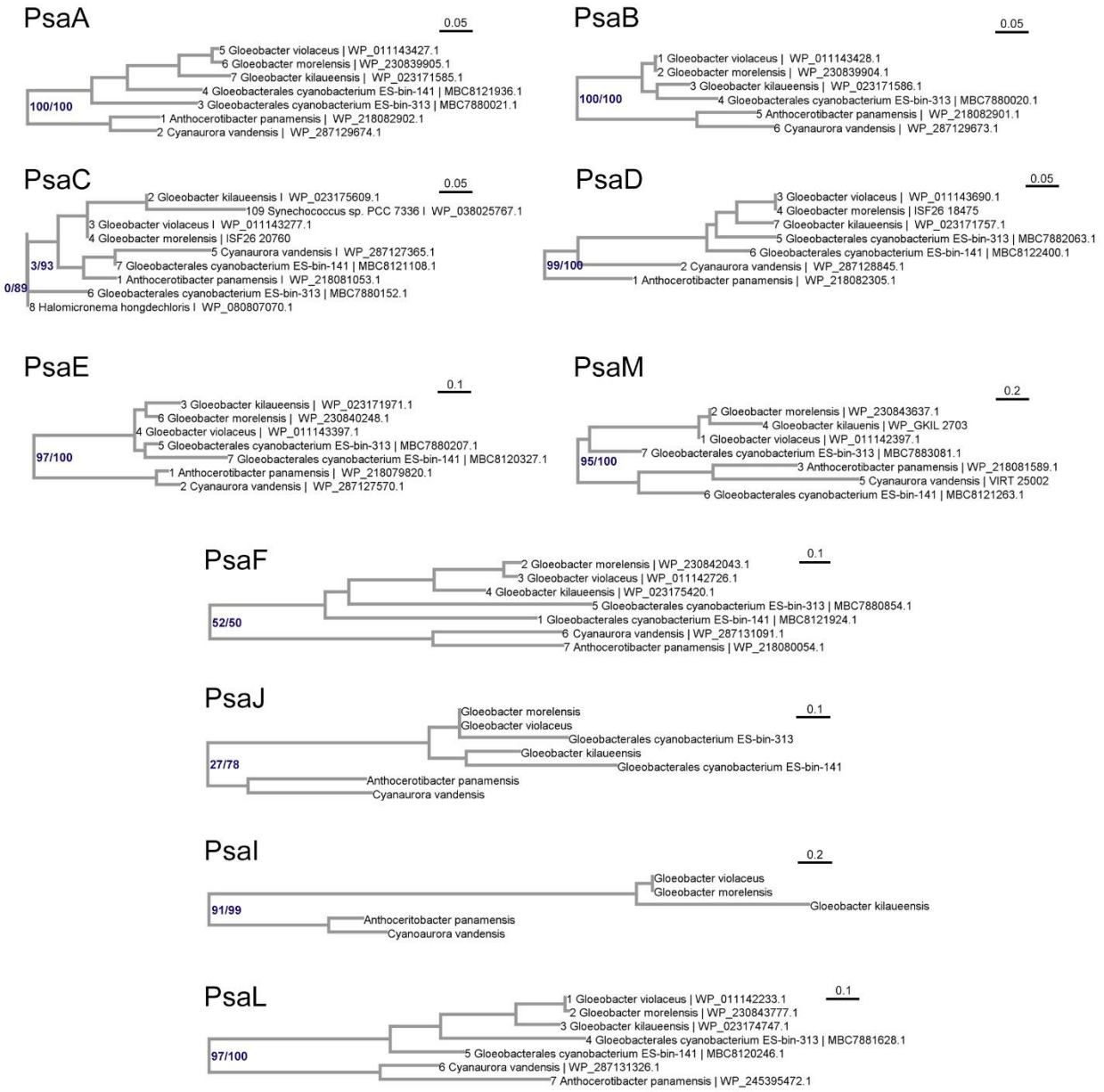

Fig. S16. Detail of PSI subunit evolution for *A. panamensis* and close relatives. Maximum Likelihood phylogenetic trees of each PSI subunit in *A. panamensis.* Trees were run as described in **Materials and Methods** and rooted at the branching point of the Gloeobacterales. Only Gloeobacterales are shown here. The trees show that PSI subunits in Gloeobacterales show strong congruence across subunits, suggesting that these have been passed down vertically since their most recent common ancestor. No evidence for replacement of subunits via horizontal gene transfer or gain of subunit paralogs via duplication is observed. Full trees and sequence alignments are provided as **Data S1**. Scale bars represent amino acids substitutions per site.

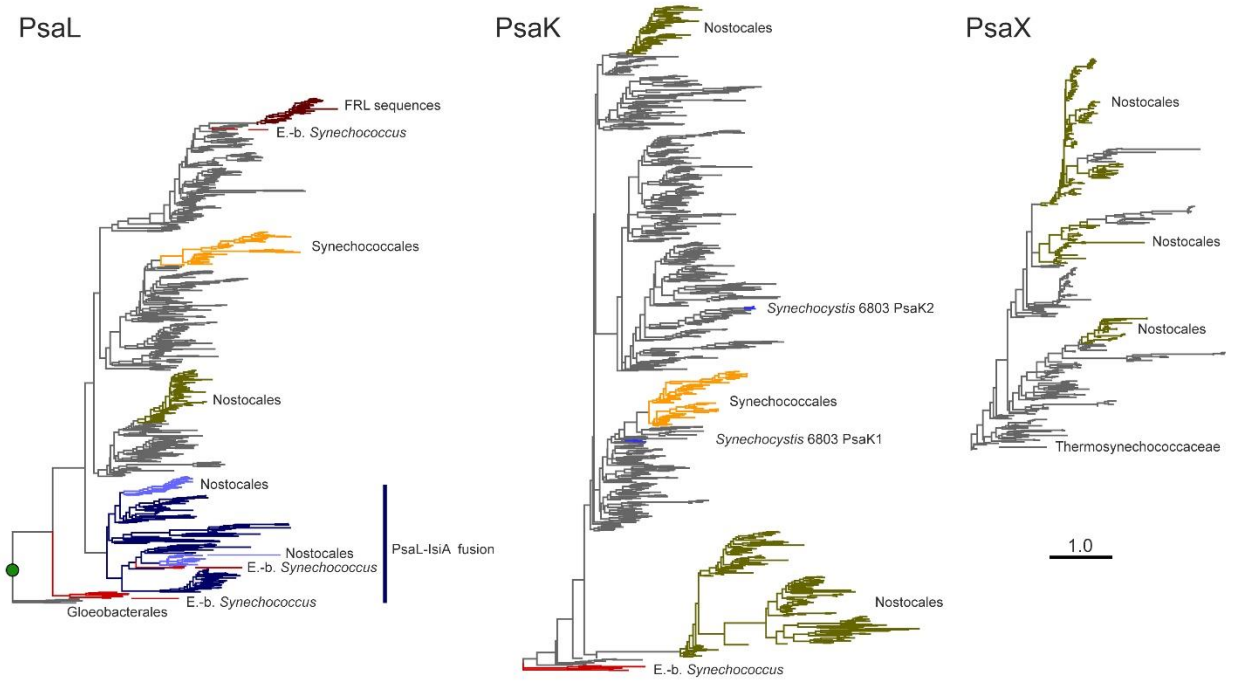

Fig. S17. Maximum Likelihood tree of PsaL, PsaK, and PsaX. The PsaL phylogeny was rooted at the branching point of the Gloeobacterales. Several gene duplications are noted, some of which appear to be very ancient. In particular, that leading to the PsaL-IsiA fusion, which likely occurred after the early divergence of the clade containing the early-branching *Synechococcus* (E.-b *Synechococcus*). The PsaL-IsiA fusion appears to have duplicated at least once as evidenced by the presence of two distinct paralogues in Nostocales (e.g. heterocystous cyanobacteria). Synechococcales denotes the *Synechococcus-Prochlorococcus* clade. FRL sequences represent another duplication leading to the paralogue found in the far-red light photoacclimation gene cluster. PsaK is absent in Gloeobacterales but it is found in most other cyanobacteria, including the early-branching *Synechococcus*, where the tree was rooted for display. Several duplications are noted as evidenced by the two paralogues found in Nostocales as well as the two paralogues known in the model cyanobacterium *Synechocystis* 6803. In contrast, PsaX has a limited distribution. It is neither found in any of the most basal cyanobacterial groups nor the Synechococcales, except for a few strains in the *Thermosynechococcus* group, where the tree was rooted for display. The subunit appears to be most widely distributed in Nostocales and their relatives, as well as other macrocyanobacteria.

Supplementary Tables

Table S1. Mass spectrometric analysis of the *A. panamensis* PSI fraction from sucrose gradient. The criteria for identifying a protein were two peptides and a false discovery rate below 0.01. The protein scores are calculated as the sum of the scores of peptides.

Protein	Score	Coverage (%)	Molecular weight (kDa)
PsaA	5,463	59	86.6
PsaB	4,590	51.8	82.8
PsaC	1,271	98.8	8.8
PsaD	3,908	95.8	15.5
PsaE	2,418	98.4	7.2
PsaF	2,669	74	19.5
PsaL	1,175	96.3	17
Heat shock protein 60 kDa family chaperone GroEL	7,032	87.9	57.8
Phycobilisome rod linker polypeptide, phycocyanin-associated (CpcN)	5,107	60.7	133.8
Phycocyanin beta chain	5,060	100	18.4
Phycocyanin alpha chain	4,742	99.4	17.8
Heat shock protein 60 kDa family chaperone GroEL	3,902	71.2	58.5
Glutamine synthetase type I (EC 6.3.1.2)	3,344	94.5	52.4
ATP synthase beta chain (EC 3.6.3.14)	2,331	78.5	51.9
Ribulose bisphosphate carboxylase large chain (EC 4.1.1.39)	1,616	61.8	52.7
ATP synthase alpha chain (EC 3.6.3.14)	1,482	64.1	54
CRISPR-associated protein, Cse4 family	1,397	58.2	41.4
hypothetical protein	1,354	46.1	88.9
Photosystem II CP47 protein (PsbB)	1,265	38.9	59.7
Protein QmcA (possibly involved in integral membrane quality control)	1,165	52.2	35.7
Phycobilisome phycoerythrin-associated linker polypeptide CpcJ	968	26.6	60.2
Branched-chain amino acid ABC transporter, substrate-binding protein LivJ (TC 3.A.1.4.1)	685	52.7	40.4
Heat shock protein 10 kDa family chaperone GroES	651	95.1	11

Table S2. Mass spectrometric identification of in-gel digested proteins from SDS-PAGE. Ten selected bands from the SDS-PAGE of PSI, labeled 1–7 in **Fig. 1e** were analyzed. The protein scores are calculated as the sum of the scores of peptides. The top four proteins with the highest scores are included. The high-molecular-weight Psa subunits detected at Band 6-7 are likely degraded proteins, indicated by their low scores and coverages. The identified PSI subunits are highlighted in green.

	Protein	Score	Coverage (%)	Molecular weight (kDa)
Band 1	PsaB	1544	25.9	82.8
	PsaA	1499	32.5	86.6
	CpcN	1446	32.5	133.8
	hypothetical protein	1308	61.7	61.1
Band 2	CpcN	484	25.5	133.8
	CpcJ	425	42.2	60.2
	SSU ribosomal protein S4p	401	63.6	23.5
	PsaB	228	14.6	82.8
Band 3	PsaD	1585	99.3	15.5
	PsaF	1478	45.8	19.5
	Phycocyanin alpha chain	742	84	17.8
	Phycocyanin beta chain	736	83.1	18.4
Band 4	PsaD	292	86.7	15.5
	PsaC	234	74.1	8.8
	PsaL	224	31.3	17
	SSU ribosomal protein S17p	174	45.1	11.5
Band 5	PsaC	666	100	8.8
	PsaE	349	98.4	7.2
	PsaF	123	21.5	19.5
	Phycocyanin alpha chain	86	30.1	17.8
Band 6	Ribulose bisphosphate carboxylase large chain	69	4	52.7
	PsaA	52	2.3	86.6
	PsaC	45	35.8	8.8
	ABC transporter, RND-adapter-like protein	36	1.4	46.7
Band 7	PsaB	81	1.7	82.8
	Ribulose bisphosphate carboxylase large chain	59	5.5	52.7
	Alanyl-tRNA synthetase	39	0.7	94.2
	PsaA	37	3.2	86.6

Table S3. Cryo-EM data collection, refinement, and validation statistics for *A. panamensis* PSI.

Data collection and processing	
Magnification	x105,000
Voltage (kV)	300
Electron exposure (e^{-}Å^{-2})	50.0
Defocus range (μm)	−0.8 to −2.2
Pixel size (Å)	0.825
Symmetry imposed	C3
Initial particle images (no.)	991,198
Final particle images (no.)	403,080
Map resolution (Å)	2.40
FSC threshold	0.143
Refinement	
Initial model used (PDB code)	7F4V
Model resolution (Å)	2.44
FSC threshold	0.5
Map resolution range (Å)	2.10-3.20
Map-sharpening *B* factor (Å^2)	−64.3
Model composition	
Non-hydrogen atoms	69,921
Protein residues	6,498
Ligands	366
B factors (Å^2)	
Protein	20
Ligands	23
R.m.s. deviations	
Bond lengths (Å)	0.009
Bond angles (°)	2.288
Validation	
MolProbity	2.48
Clashscore	10.63
Rotamer outliers (%)	4.62
Ramachandran plot	
Favored (%)	93.40
Allowed (%)	5.78
Disallowed (%)	0.82

Table S4. Cryo-EM model composition (per monomer).

	Number
Protein subunits	10
Chlorophyll *a*	88
Chlorophyll *a'*	1
Menaquinone-4	2
β-carotene	22
Echinenone	1
[4Fe-4S] cluster	3
Phosphatidylglycerol	3
Distearoyl-monogalactosyl-diglyceride	1
***n*-dodecyl β-D-maltoside**	1

Table S5. Sequence identities and root-mean square deviation (RMSD) of *A. panamensis* PSI subunits with those from other selected cyanobacterial species for which structures are available. Values are colored from green to white corresponding to most to least similar.

	Sequence Identity (%)	RMSD (Å)
PsaA		
G. violaceus	76.74	0.400
T. vestitus	73.73	0.501
Synechocystis 6803	72.76	0.441
PsaB		
G. violaceus	79.92	0.380
T. vestitus	74.07	0.454
Synechocystis 6803	76.56	0.438
PsaC		
G. violaceus	96.30	0.302
T. vestitus	92.59	0.362
Synechocystis 6803	93.83	0.356
PsaD		
G. violaceus	79.72	0.304
T. vestitus	57.97	0.486
Synechocystis 6803	58.70	0.452
PsaE		
G. violaceus	75.00	0.407
T. vestitus	61.90	0.400
Synechocystis 6803	58.73	0.330

	Sequence Identity (%)	RMSD (Å)
PsaF		
G. violaceus	36.90	0.634
T. vestitus	39.07	0.881
Synechocystis 6803	35.53	0.981
PsaI		
G. violaceus (PsaZ)	53.12	0.240
T. vestitus	29.03	0.662
Synechocystis 6803	31.25	0.742
PsaJ		
G. violaceus	17.50	0.395
T. vestitus	28.21	1.086
Synechocystis 6803	26.32	1.064
PsaL		
G. violaceus	54.42	0.717
T. vestitus	42.18	2.246
Synechocystis 6803	43.92	0.993
PsaM		
G. violaceus	58.06	0.415
T. vestitus	38.71	0.798
Synechocystis 6803	38.71	0.842

Data S1. Phylogenetic trees and sequence alignments used for Fig. S16. (external)